Radiative Jeffrey fluid transport over a stretching surface with anomalous heat and mass flux

Article *in* International Journal of Modern Physics B · September 2023

DOI: 10.1142/S0217979224503508

4 authors, including:

Kazeem B. Kasali
First Technical University
8 PUBLICATIONS **47** CITATIONS
SEE PROFILE

Yusuf Olatunji Tijani
33 PUBLICATIONS **247** CITATIONS
SEE PROFILE

Yusuf Abdulhakeem
Federal University of Technology Minna
26 PUBLICATIONS **32** CITATIONS
SEE PROFILE

International Journal of Modern Physics B
(2024) 2450350 (20 pages)

DOI: 10.1142/S0217979224503508

World Scientific
www.worldscientific.com

Radiative Jeffery fluid transport over a stretching surface with anomalous heat and mass flux

Kazeem B. Kasali*
*Department of Mathematics and Statistics, First Technical University, Ibadan

Yusuf O. Tijani†
†Department of Mathematics and Applied Mathematics,
Nelson Mandela University, Port-Elizabeth, South Africa

Suraju O. Ajadi‡
‡Department of Mathematics, Obafemi Awolowo University, Ile-Ife, Nigeria

Abdulhakeem Yusuf§,¶
§Department of Mathematics Federal University of
Technology Minna, Niger State Nigeria
¶olodyusuf@gmail.com

Received 14 April 2023
Revised 20 June 2023
Accepted 21 June 2023
Published

As a means of influencing technological advancements in engineering applications and various fluid products, the generalized Fourier's and Fick's models have proven to be of great importance. Industries such as power station engineering, high thermal material processing, and bio-heat elements apply the concept of anomalous heat and mass transfer mechanism. The objective of this study is to stimulate the flow of a radiative magnetohydrodynamics Jeffery fluid over an expanding surface with anomalous heat and mass transfer dynamics subjected to nth order reaction and variable thermophysical properties. A set of similarity transformations is used to neutralize the governing equations into a nondimensionless form. To obtain the model parametric analysis, a numerical tool via the spectral local linearization method (SLLM) is deployed after transformation of the governing flow equation from a two-unknown partial differential equations to a one-variable ordinary differential equation. It is observed that the thermal boundary layer thickness is found to be enhanced with increasing parametric values of magnetic, Eckert and radiation parameters. For the radiation parameter $R \in [0.50, 2.50]$, the skin drag force, Nusselt and Sherwood number increase by 0.61%, 48.00% and 0.91%, respectively. Additionally, a 200% increment in the nth order parameter boosts the rate of heat transfer by 0.78%. while it downsizes the Sherwood number by 14.32%.

Keywords: Jeffrey fluid; thermal radiation; chemical reaction; Catteneo–Christov; stretching surface; MHD.

PACS numbers:

Nomenclatures

P_r	Prandtl number
M	Magnetic parameter
K_r'	Chemical reaction parameter
R	Radiation parameter
E_c	Eckert number
c_p	Specific heat capacity
g	Acceleration due to gravity
T	Temperature of the fluid
x, y	Cartesian coordinates
u	Velocity component in the x-axis
S_c	Schmidt number
D_0	Ambient Brownian diffusion coefficient
Gr	Thermal Grashof number
Gc	Solutal Grashof number
$k(T)$	Temperature-dependent thermal conductivity
k_0	Thermal conductivity of the ambient temperature
$D_m(C)$	Space-dependent molecular diffusivity
$\mathbf{V}$	Velocity vector
$\mathbf{q}$	Heat flux vector
q_r	Radiation
q_w	Heat flux
q_m	Mass flux
$\mathbf{J}$	Electric current density
n	Order of chemical reaction
p	Pressure
f	Dimensionless velocity
C	Concentration of the fluid
v	Velocity component in the y-axis
c	Stretching coefficient
Re_x	Reynolds number
k'	Mean absorption coefficient
	Greek symbols
β	Deborah number
Φ	Dissipation term
ϵ_0	Thermal conductivity parameter (-)
ϵ_1	Space diffusivity parameter
θ_w	Dimensionless temperature ratio
ρ	Fluid density
ν	Kinematic viscosity
λ_T	Thermal relaxation time
λ_C	Solutal relaxation time

λ_1, λ_2	Jeffrey fluid parameters
Λ	Unitless thermal relaxation time
Λ_0	Unitless solutal relaxation time
θ	Dimensionless temperature
ϕ	Dimensionless concentration
ψ	Stream function
∇	Gradient operator
ξ	Transform independent variable
σ'	Stefan–Boltzman constant
μ	Dynamic viscosity
β_T	Thermal diffusivity
β_C	Molar diffusivity
	Subscript
w	Wall
∞	Far field
x	Local

1. Introduction

Several industrially applied fluids, including blood, shampoo, glues, inks, slurries, paints, ketchup and polymer solutions, exhibit non-Newtonian properties. These liquids typically exhibit both viscous and elastic properties, and their behavior is inherently nonlinear. Consequently, the constitutive equations governing these fluids are more complex compared to those of typical Newtonian fluids described by the Navier–Stokes equations. The majority of non-Newtonian models, such as the Maxwell, Walters-B short memory, Eyring–Powell, Oldroyd-B and Jeffrey models, involve different levels of enhancement to the traditional momentum equation. Among these models, the Jeffrey model is known for its simplicity and is considered a straightforward type of non-Newtonian fluid. It exhibits high shear viscosity, shear-thinning behavior and yield stress characteristics.

It has been established that the Jeffrey fluid model is one of the most significant non-Newtonian fluid models that accurately describes the viscoelastic properties of fluids.[1–3] It is recognized that linear viscoelastic fluids naturally have well-defined Jeffrey fluid models. In the polymer industry, diluted polymers are a common application for Jeffrey fluids, as highlighted by Farooq *et al.*[4] and Ara *et al.*[5] The practical importance of this model equation in fluid dynamics stems from the viscoelastic behavior exhibited by Jeffrey fluids.[6]

Several MHD applications have their roots in physiology, such as the employment of magnetic particles and magnetic devices in magnetic resonance, magnetic transferors and production of bio-magnetic fluid (blood) due to presence of molecules in hemoglobin.[7] Hayat *et al.*[8,9] examined the velocity behaviors with the influence of inbuilt factors while studying MHD flow of Jeffrey fluid with various conditions. Jeffrey fluid flow across a wall with permeability was explored by Sana *et al.*[10]

The stagnation point flow of MHD Jeffrey fluid over a radially stretching sheet was presented by Hayat *et al.*[11] Flow of MHD with radiative Jeffrey fluid over a stretching sheet with a slippery surface and melting heat transfer was described by Das *et al.*[12] The magnitude of the microorganism motile density is seen to be damped for various examined thermophysical parameters in Shamshuddin *et al.*'*s*[13] investigation of the influence of magnetism on the stream bioconvection nanoliquid via porous media under the influence of heat radiation driven by stretching surface. With dual stratification, Shamshuddin *et al.*[14] developed a model for free convective chemically reacting magnetized Buongiorno nanofluid flow along a stretching exponential Riga plate. They found that increasing the magnetization parameter also increased the drag force and wall heat transfer rate. For a hydromagnetic flow down an infinite flat plate in the presence of thermal radiation and heat dissipation, Asmat *et al.*[15] addressed Stokes's second problem. Their findings show that an increase in the Prandtl number and radiation value increased the wall heat gradient profiles in a proportional manner. Moreover, efforts on MHD fluid flow problem have been discussed by various authors in Refs. 16–18.

A variety of chemical reaction systems involve both heterogeneous and homogeneous reactions. In the absence of a catalyst, certain reactions may proceed slowly or not at all. Correlating homogeneous and heterogeneous reactions poses a particular challenge due to the varying rates at which reactants are produced and consumed, both within the fluid and on the surfaces of catalysts. Food processing, hydrometallurgical industries, polymer manufacturing, chemical processing equipment design, fog generation and dispersion, crop loss from freezing, and fruit tree groves are some of the industries and applications that heavily rely on the effects of chemical reactions. Merkin[19] investigated the flow of a viscous fluid over a plate with homogeneous–heterogeneous reactions. Chaudhry and Merkin[20] conducted an examination of the boundary layer flow of a viscous fluid in the presence of homogeneous–heterogeneous processes. Homogeneous–heterogeneous interactions with point of stagnation towards a moving sheet were examined by Bachok *et al.*[21] Study of homogeneous–heterogeneous effects on viscoelastic fluid near a moving wall was presented by Khan and Pop.[22] Kameswaran *et al.*[23] discussed the study of nanofluid flow through a stretching porous medium with the inclusion of homogeneous-heterogeneous reactions. By exploring the Soret and Dufour phenomenon, Israr-Ur-Rehman *et al.*[24] examined the chemical reaction and magnetohydrodynamic mixed-convection fluid flow caused by a moveable thin needle. They found that an increase in chemical reaction causes a decline in the concentration field.

The mechanism of heat transfer holds significant importance in engineering and industrial applications, including nuclear reactors, biomedical devices, and energy space cooling. Examples of such applications include magnetic drug delivery, heat conduction in tissues, and various other areas. The conventional Fourier heat conduction equation is widely employed to describe the process of heat transmission.[25] The production of parabolic energy equation is the main setback which suggests the process under study experiences the initial disturbance immediately.

This characteristic is called paradox of heat conduction in the literature. In order to address this issue, some researchers have proposed modifications to the Fourier conduction law. One such modification was suggested by Cattaneo,[26] which involves introducing a relaxation time to the heat flow. The relaxation time represents the time required for heat conduction to be established in the system. In addition to the modification proposed by Cattaneo–Christov,[27] further changes were made to the equation by substituting the Oldroyd B convected derivative for the standard derivatives. This modification was aimed at improving the accuracy and applicability of the equation in describing heat conduction phenomena. Theoretical elements of Cattaneo–Christov heat transfer phenomenon for Reiner–Philippoff liquid stream in the presence of Darcy–Forchheimer media are presented by Israr Ur Rehman *et al.*[28] When nonlinear heat radiation, viscous dissipation, and Ohmic heating occur, the process of heat transport is eliminated. It was observed that increasing the Reiner–Philippoff fluid parameter and Forchheimer number results in an enhancement of the velocity curve. On the other hand, increasing the thermal relaxation parameter and Eckert scales leads to a decrease in the rate of heat transfer at the surface. The effects of Cattaneo–Christov heat fluxing on the Darcy–Frochheimer flow of Sutterby nanofluid via stretchable surface with chemical reactive and heat radiative impacts were examined by Israr Ur Rehman *et al.*[29] As the Forchheimer number increases, both the skin friction and velocity curve decrease. Christov and Cattaneo heat models are used in conjunction to study the thermal convection effect in Alamri *et al.*[30] The incompressible fluid responses of Cattaneo–Christov heat conduction model were studied by Tibullo and Zampoli.[31] With the effect of gravity, Straughan[32] studied the horizontal layer Newtonian incompressible fluid with Cattaneo–Christov thermal convection. Stability of the structure and inequality of Cattaneo–Christov model were investigated by Ciarletta and Straughan.[33] Non-Fourier heat conduction dynamical analysis and its use in nanosystems were explored by Dong *et al.*[34] Heat flux model of Cattaneo–Christov in Maxwell fluid flow was described in Han *et al.*[35] Mustafa[36] discussed Maxwell fluid upper convective flow with rotation and a Cattaneo–Christov heat flux. Ashraf *et al.*[37] performed the computational analysis of Cattaneo–Christov heat flux on MHD Jeffrey fluid.

A stretching sheet, also known as a moving or translating sheet, refers to a surface over which a fluid flows. The stretching sheet problem is of interest in both theoretical and applied research. The observation noted in stretchable surfaces and the corresponding flow field behavior indicates their potential applications in various technological and industrial sectors. These include paper production, glass manufacturing, crystal formation, and the extrusion of aerodynamic plastic sheets, see Hayat *et al.*[38] According to Xiu *et al.*,[39] the combined effects of the Lorentz force, micro-rotation, and particle thermo-migration on the dynamics of micropolar fluids subjected to nonlinear thermal radiation and the Arrhenius chemical reaction connected to the activation energy were the main focus of their research. The study revealed that the micro-rotation field is dominated by a small number of particle

spins generated by boundary collisions. Tijani *et al.*[40] analyzed the generalized heat and mass flux model on Casson and Williamson fluid over an expanding Riga surface. For more study in this direction, the reader is advised to see the investigation conducted in Refs. 41 and 42.

Several scholars have shown interest in conventional numerical schemes like finite difference method (FDM) and finite element method (FEM) for computationally solving the fluid flow model. However, there is a growing body of researchers who are dedicated to developing novel numerical techniques that can surpass the limitations associated with traditional approaches, particularly in terms of time efficiency, accuracy and rate of convergence. Rai and Mondal[43] observed the spectral methods such as spectral homotopy analysis method (SHAM), successive linearization method (SLM), spectral local linearization method (SLLM), spectral quasi-linearization method (SQLM), and spectral multi domain quassilinearization method (SMDQM) to mention but few. The SLLM combines elements of spectral methods and local linearization to achieve accurate and efficient solutions for linear/nonlinear differential equations. The SLLM offers several advantages; it can handle highly nonlinear systems with accuracy and has been shown to have a quadratic convergence. ~~Using this spectral numerical technique, Shateyi and Marewo[44] investigated the movement of warm on a porous medium that expands temporally, following the suggestion made by Motsa.~~[45] In order to comprehend nanofluid stream two-dimensional flow across a warmed nonhorizontal surface with a sinusoidal temperature, Motsa and Awad[46] adopted the spectral local linearization method. The study conducted by Mosta *et al.*[47] and Sithole *et al.*[48] provides valuable insights into the utilization and application of the spectral local linearization method (SLLM).

The novelty of this research is that no other study has examined the Catteneo–Christsov heat and generalized Fick's mass transfer phenomena on Jeffery fluid subject to nth order chemical reaction and variable thermophysical properties, at least, not to the author's knowledge. This study aims at understanding the impacts of chemical reaction and variable thermophysical properties on dissipative Jeffery fluid with MHD effect through a two-dimensional stretched sheet. Objectives of the study include: (i) the model of the 2D Jeffery fluid, (ii) transformation of the governing PDEs to systems of ODEs via an appropriate similarity variables, (iii) implementation of spectral local linearization method (SLLM) on the formulated problem and (iv) investigating the behavior of the pertinent flow parameters via graphs and tables.

2. Mathematical Model

By considering a two-dimensional steady flow of an incompressible magnetohydrodynamics Jeffrey fluid over a linearly stretching sheet with nonconstant thermal conductivity and variable mass diffusivity, the effects of thermal radiation, reaction dynamics, and viscous dissipation are analyzed on the flow. The expansion of the surface is related to the function $u = cx$, and the magnetic field acting in the flow

direction is nonuniformly transverse with a strength of $B = B_0 x^{-\frac{1}{2}}$, where the induced magnetic field is negligible due to a low magnetic Reynolds number. The analysis includes the utilization of the full form of the nonlinear thermal radiative heat flux, without truncation of higher-order terms in the expansion. The heat and mass transfer phenomena exhibit deviations from the classical models of Fourier's heat transfer and Fick's mass transfer. Under these assumptions, the conservation equations are given as follows:

$$\nabla \cdot \mathbf{V} = 0, \tag{2.1}$$

$$\rho[(\mathbf{V} \cdot \nabla)\mathbf{V}] = \nabla \cdot \tau + \mathbf{J} \times \mathbf{B} + \rho \mathbf{g}, \tag{2.2}$$

$$\rho c_p[(\mathbf{V} \cdot \nabla)T] = -\nabla \cdot \mathbf{q} - \frac{\partial \mathbf{q_r}}{\partial \mathbf{y}} + \mathbf{J} \times \mathbf{B}, \tag{2.3}$$

$$(\mathbf{V} \cdot \nabla)C = -\nabla \cdot \mathbf{j} - \mathbf{k_r}(\mathbf{C} - \mathbf{C}_\infty)^{\mathbf{n}}, \tag{2.4}$$

τ is the constitutive stress relation for Jeffrey fluid and it is given by

$$\tau = -pI + \frac{\mu}{1+\lambda_1}[(\nabla \mathbf{V} + (\nabla \mathbf{V})^j) + \lambda_2 \frac{d}{dt}(\nabla \mathbf{V} + (\nabla \mathbf{V})^j)]. \tag{2.5}$$

The heat and mass flux models employed using the Cattaneo–Christov models are given as follows.[27,51]

$$\mathbf{q} + \lambda_T \left(\frac{\partial \mathbf{q}}{\partial t} + \mathbf{V} \cdot \nabla \mathbf{q} - \mathbf{q} \cdot \nabla \mathbf{V} + (\nabla \cdot \mathbf{V})\mathbf{q} \right) = -k(T)\nabla T, \tag{2.6}$$

$$\mathbf{j} + \lambda_C \left(\frac{\partial \mathbf{j}}{\partial t} + \mathbf{V} \cdot \nabla \mathbf{j} - \mathbf{j} \cdot \nabla \mathbf{V} + (\nabla \cdot \mathbf{V})\mathbf{j} \right) = -D_m(C)\nabla C. \tag{2.7}$$

Essentially, when $\lambda_T = 0$ and $\lambda_C = 0$, Eqs. (2.6) and (2.7) reduce to classical heat flux and mass flux, respectively. By applying the conditions of steadiness and incompressibility to the fluid flow, Eqs. (2.6) and (2.7), respectively, reduce to

$$\mathbf{q} + \lambda_T(\mathbf{V} \cdot \nabla \mathbf{q} - \mathbf{q} \cdot \nabla \mathbf{q}) = -K(T)\nabla T, \tag{2.8}$$

$$\mathbf{j} + \lambda_C(\mathbf{V} \cdot \nabla \mathbf{j} - \mathbf{j} \cdot \nabla \mathbf{q}) = -D_m(C)\nabla C. \tag{2.9}$$

Using the boundary layer approximation, Eqs. (2.1)–(2.9) can be expressed in the component form with respect to the variables (x, y) as follows:

$$\frac{\partial u}{\partial x} + \frac{\partial v}{\partial y} = 0, \tag{2.10}$$

$$u\frac{\partial u}{\partial x} + v\frac{\partial u}{\partial y} = \frac{\nu}{1+\lambda_1}\left[\frac{\partial^2 u}{\partial y^2} + \lambda_2\left(u\frac{\partial^3 u}{\partial x \partial y^2} - \frac{\partial u}{\partial x}\frac{\partial^2 u}{\partial y^2} + \frac{\partial u}{\partial y}\frac{\partial^2 u}{\partial x \partial y} + v\frac{\partial^3 u}{\partial y^3}\right)\right] + g\beta_T(T - T_\infty) + g\beta_C(C - C_\infty) - \frac{\sigma B_0^2 u}{\rho}, \tag{2.11}$$

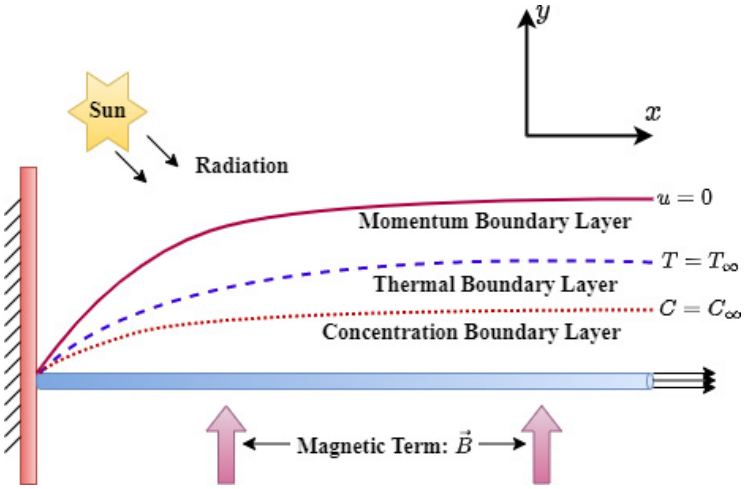

Fig. 1. (Color online) Flow configuration.

$$u\frac{\partial T}{\partial x}+v\frac{\partial T}{\partial y}+\lambda_T\Omega_T=\frac{1}{\rho c_p}\frac{\partial}{\partial y}\left(k(T)\frac{\partial T}{\partial y}\right)+\frac{\nu}{c_p(1+\lambda_1)}\times\left[\left(\frac{\partial u}{\partial y}\right)^2+\lambda_2\left(u\frac{\partial u}{\partial y}\frac{\partial^2 u}{\partial x\partial y}+v\frac{\partial u}{\partial y}\frac{\partial^2 u}{\partial y^2}\right)\right]+\frac{\sigma B_0^2u^2}{\rho c_p}-\frac{1}{\rho c_p}\frac{\partial q_r}{\partial y}, \tag{2.12}$$

$$u\frac{\partial C}{\partial x}+v\frac{\partial C}{\partial y}+\lambda_0\left[\left(u\frac{\partial u}{\partial x}+v\frac{\partial u}{\partial y}\right)\frac{\partial C}{\partial x}+\left(u\frac{\partial v}{\partial x}+v\frac{\partial v}{\partial y}\right)\frac{\partial C}{\partial y}+u^2\frac{\partial^2 C}{\partial x^2}+v^2\frac{\partial^2 C}{\partial y^2}+2uv\frac{\partial^2 C}{\partial x\partial y}\right]=\frac{\partial}{\partial y}\left(D_m(C)\frac{\partial C}{\partial y}\right)-k_r(C-C_\infty)^n. \tag{2.13}$$

Here, $\Omega_T=u^2\frac{\partial^2 T}{\partial x^2}+\left(u\frac{\partial u}{\partial x}+v\frac{\partial u}{\partial y}\right)\frac{\partial T}{\partial x}+v^2\frac{\partial^2 T}{\partial y^2}+\left(u\frac{\partial v}{\partial x}+v\frac{\partial v}{\partial y}\right)\frac{\partial T}{\partial y}+2uv\frac{\partial^2 T}{\partial x\partial y}$.

The conditions of flow at the wall and far-field are (Akinbobola and Okoya[57]);

$$u=u_w(x)=cx,\quad v=0,\quad C=C_w,\quad T=T_w,\quad \text{at } y=0, \tag{2.14}$$

$$T\to T_\infty,\quad u\to 0,\quad \frac{\partial u}{\partial y}\to 0,\quad C\to C_\infty\quad \text{as } y\to\infty. \tag{2.15}$$

The temperature-function thermal conductivity $k(T)$ and specie-dependent molecular diffusivity $D_m(C)$ are given as (Tijani *et al.*[58])

$$k(T)=K_0\left(1+\epsilon_0\left(\frac{T-T_\infty}{T_w-T_\infty}\right)\right)\quad D_m(C)=D_0\left(1+\epsilon_1\left(\frac{C-C_\infty}{C_w-C_\infty}\right)\right). \tag{2.16}$$

With the aid of similarity variables,

$$\xi(x,y)=\sqrt{\frac{c(1+\lambda_1)}{\nu}}y,\quad \psi(x,y)=\sqrt{\frac{c\nu}{1+\lambda_1}}xf(\xi),\\ \theta(\xi)=\frac{T-T_\infty}{T_w-T_\infty},\quad \phi(\xi)=\frac{C-C_\infty}{C_w-C_\infty}. \tag{2.17}$$

Equations (2.10)–(2.15) become

$$f'''+ff''+\beta(f''^2-ff'')-Mf'+Gr\theta-f'^2+Gc\phi=0, \tag{2.18}$$

$$(1+\lambda_1)\Big[(1+\epsilon_0\theta)\theta''+\epsilon_0(\theta')^2+\frac{4}{3}R(3(\theta_w-1)(1+(\theta_w-1)\theta)^2\theta'^2\\ +(1+(\theta_w-1)\theta)^3\theta'')\big]+P_rf\theta'+E_cP_r[(f'')^2+\beta(f'f''^2-ff''f''')\\ +Mf'^2]-\Lambda P_r(ff'\theta'+f^2\theta'')=0. \tag{2.19}$$

$$(1+\lambda_1)[(1+\epsilon_1\phi)\phi''+\epsilon_1(\phi')^2]-S_ck_r'\phi^n+S_cf\phi'-S_c\Lambda_0(ff'\phi'+f^2\phi'')=0. \tag{2.20}$$

Note that the continuity Eq. (2.10) is automatically satisfied. The applicable boundary conditions are neutralized to the subsequent ones, given as follows:

$$\xi=0,\quad f(\xi)=0,\quad f'(\xi)=1,\quad \phi(\xi)=1,\quad \theta(\xi)=1,\\ \xi\to\infty,\quad f'(\xi)\to0,\quad \phi(\xi)\to0,\quad f''(\xi)\to0,\quad \theta(\xi)\to0. \tag{2.21}$$

with the given nondimensional physical parameter

$$\begin{cases} P_r=\dfrac{\mu c_p}{\kappa},\quad M=\dfrac{\sigma B_0^2}{\rho c},\quad k_r'=\dfrac{k_r(C-C_\infty)^{n-1}}{c},\quad \Lambda_0=\lambda_Cc,\quad E_c=\dfrac{u^2}{c_p(T_w-T_\infty)},\\ R=\dfrac{4\sigma'T_\infty^3}{k'k},\quad \Lambda=\lambda_Tc,\quad S_c=\dfrac{D_m}{\nu},\quad \beta=\lambda_2c,\quad Gr=\dfrac{g\beta_T(T_w-T_\infty)}{cu_w},\\ Gc=\dfrac{g\beta_C(C_w-C_\infty)}{cu_w}. \end{cases} \tag{2.22}$$

The engineering quantities of the surface drag force, Nusselt and Sherwood numbers are defined as

$$C_f=\frac{\tau_w}{\rho u_w^2},\quad Nu_x=\frac{xq_w}{k_0(T_w-T_\infty)},\quad Sh_x=\frac{xq_m}{D_0(C_w-C_\infty)}, \tag{2.23}$$

where τ_w, q_w and q_m are given as

$$\tau_w=\frac{\mu}{1+\lambda_1}\left[\frac{\partial u}{\partial y}+\lambda_2\left(u\frac{\partial^2u}{\partial x\partial y}+v\frac{\partial^2u}{\partial y^2}\right)\right]\Big|_{y=0},\\ q_w=-\left(k(T)+\frac{16\sigma'}{3k'}T^3\right)\frac{\partial T}{\partial y}\Big|_{y=0},\quad q_m=-D_m(C)\frac{\partial C}{\partial y}\Big|_{y=0}. \tag{2.24}$$

With the aids of Eqs.(2.17), (2.22) and (2.24), the nondimensional form of Eq. (2.23) becomes

$$\begin{aligned}
\mathrm{Re}_x^{\frac{1}{2}} C_f &= \frac{\beta}{1+\lambda_1}\left[\frac{f''(0)}{\beta} + (-f(0)f'''(0) + f'(0)f''(0))\right],\\
\mathrm{Re}_x^{-\frac{1}{2}} Sh_x &= -[1+\epsilon_1\phi(0)]\phi'(0),\\
\mathrm{Re}_x^{-\frac{1}{2}} Nu_x &= -\left[1+\epsilon_0\theta(0) + \frac{4}{3}R(1+(\theta_w-1)\theta(0))^3\right]\theta'(0).
\end{aligned} \tag{2.25}$$

Here, $\mathrm{Re}_x = \frac{(1+\lambda_1)xu_w}{\nu}$ stands for Reynolds number.

3. Method of Solution

Equations (2.18)–(2.20) with its suitable conditions enlisted in Eq. (2.21) will be solved using a numerical approach of the spectral kind. The spectral local linearization method (SLLM) which is due to the work of Motsa[45] is the numerical means of solution here. The method works by locally linearizing our variable of interest before computing them iteratively. The local linearization technique is credited to Bellman and Kalaba,[60] which can be seen as an extension of the Newton–Raphson approach. For more study of this method, the reader can consult the following work — Ogunseye *et al.*[61] The local linearization takes the form

$$\Omega_{1,g} f''''_{(g+1)} + \Omega_{2,g} f'''_{(g+1)} + \Omega_{3,g} f''_{(g+1)} + \Omega_{4,g} f'_{(g+1)} + \Omega_{5,g} f_{(g+1)} = R_{f_1}, \tag{3.1}$$

$$\Omega_{6,g}\theta''_{(g+1)} + \Omega_{7,g}\theta'_{(g+1)} + \Omega_{8,g}\theta_{(g+1)} = R_{f_2}, \tag{3.2}$$

$$\Omega_{9,g}\phi''_{(g+1)} + \Omega_{10,g}\phi'_{(g+1)} + \Omega_{11,g}\phi_{(g+1)} = R_{f_3}, \tag{3.3}$$

as well as appropriate boundary conditions

$$\begin{aligned}
&\xi = 0, \quad f'_{(g+1)} = 1, \quad f_{(g+1)} = 0, \quad \phi_{(g+1)} = 1, \quad \theta_{(g+1)} = 1,\\
&\xi \to \infty, \quad f''_{(g+1)} = 0, \quad \phi_{(g+1)} = 0, \quad f'_{(g+1)} = 0, \quad \theta_{(g+1)} = 0
\end{aligned} \tag{3.4}$$

and the variable (coefficient) given as

$$\begin{cases}
\Omega_{1,g} = -\beta f, \quad \Omega_{2,g} = 1, \quad \Omega_{3,g} = 2\beta f'' + f, \quad \Omega_{4,g} = -2f' - M,\\
\Omega_{5,g} = -\beta f'''' + f'', \ \Omega_{6,g} = (1+\lambda_1)\left(\epsilon\theta + 1 + \frac{4}{3}R(1+(\theta_w-1)\theta)^3\right) - \Lambda Prf^2,\\
\Omega_{7,g} = (1+\lambda_1)(2\epsilon\theta' + 8R(1+(\theta_w-1)\theta)^2(\theta_w-1)\theta) + Prf - \Lambda Prff',\\
\Omega_{8,g} = (1+\lambda_1)\left[\epsilon\theta'' + \frac{4}{3}R((6(1+(\theta_w-1)\theta))(\theta_w-1)^2\theta'^2\right.\\
\qquad \left. + 3(1+(\theta_w-1)\theta)^2\theta''(\theta_w-1))\right],\\
\Omega_{9,g} = (1+\lambda_1)(\epsilon_1\phi+1) - S_c\Lambda_0 f^2, \quad \Omega_{10,g} = (2(1+\lambda_1))\epsilon_1\phi' + S_c f - S_c\Lambda_0 ff',\\
\Omega_{11,g} = (1+\lambda_1)\epsilon_1\phi'' - \dfrac{S_c K r \phi^n n}{\phi}
\end{cases} \tag{3.5}$$

and residuals

$$\begin{cases} R_{f_1} = \Omega_{1,g} f'''_{(g)} + \Omega_{2,g} f'''_{(g)} + \Omega_{3,a} f''_{(a)} + \Omega_{4,g} f'_{(g)} + \Omega_{5,g} f_{(g)} - P_1, \\ R_{f_2} = \Omega_{6,g} \theta''_{(g)} + \Omega_{7,a} \theta'_{(g)} + \Omega_{8,a} \theta_{(g)} - P_2, \\ R_{f_3} = \Omega_{9,a} \phi''_{(g)} + \Omega_{10,a} \phi'_{(g)} + \Omega_{11,a} \phi_{(g)} - P_3, \end{cases} \tag{3.6}$$

where P_1, P_2 and P_3 represent Eqs. (2.18), (2.19) and (2.20), respectively. The following appropriate functions are chosen as initial guesses to the iterative scheme:

$$f_{1(g)} = 1 - e^{-\xi}, \quad \theta_{2(g)} = e^{-\xi} \quad \text{and} \quad \phi_{(g)} = e^{-\xi}. \tag{3.7}$$

For brevity, the other numerical procedure can be found in Refs. 54, 59, 61 and 62. The numerical method algorithm is given as follows.

1. Define the number of grid points.
2. Define differentiation matrix.
3. Map the physical domain $[0, \infty]$ to the computational domain $[-1, 1]$ using the appropriate linear transformation.
4. Transform the differentiation matrix and define as variable **D**.
5. Define higher order derivatives: $\mathbf{D}^2$, $\mathbf{D}^3$.
6. Define initial guesses for the solutions.
7. Define total number of iterations: *iter_no*
8. **for** $\{q = 0, 1, 2, \ldots\}$
9. Define matrix system for the equations.
10. Insert boundary conditions for the equations.
11. Solve the system by matrix inversion.
12. Update solutions.
13. Update the derivatives of the solutions.
14. **If** $q ==$ iter_no
15. **end for**
16. **Else** {
17. Repeat {steps 9–13}}
18. **End if**
19. **End for**

3.1. *Numerical validation*

In this section, the convergence and agreement of the numerical method with previously published work in literature is simply brought to light.

Table 1 illustrates the convergence analysis of the spectral local linearization method (SLLM). It is observed that the difference in the numerical solution between the fourth and sixth iterations is approximately less than 10^{-11} tolerance. As expected for convergence, this implies that the difference in consecutive solutions tends to zero as the number of iterations increases. Thus, the numerical method can be deemed fit to provide reasonable approximate solution to the differential

Table 1. Convergence investigation of the SLLM with 50 collocation points using the following parametric values of $R = 2.5$, $Gr = 0.1$, Gc $= 0.1$, Pr $= 7.2$, $\lambda_1 = 0.3$, $\varepsilon = 0.5$, $\theta_w = 1.5$, $\Lambda = 0.4$, $\epsilon = 0.2$, $S_c = 1.2$, $\Lambda_0 = 1.0$, Kr $= 0.2$, $n = 1.0$, $\beta = 0.1$, $M = 2.5$, $Ec = 0.1$.

Iterations	SLLM		
r	$f''(0)$	$\theta'(0)$	$\phi'(0)$
1.0	−1.700441224994433	−0.168517805627831	−0.581392551860955
4.0	−1.700441834753811	−0.168551433543415	−0.581404634158543
6.0	−1.700441834720033	−0.168551433543070	−0.581404634156882

Table 2. $-f''(0)$ for variation of M when $Gc = Gr = \beta = 0$.

M	$-f''(0)$			
	Lawal *et al.*[54]	Alsaedi *et al.*[63]	Naseem *et al.*[64]	Current
0.0	1.00000	1.00000	1.00000	1.000000
0.5	1.11803	1.11803	1.11802	1.118033
1.0	1.41421	1.41421	1.41420	1.414213

equations given in Eqs. (2.18)–(2.20) with its boundary conditions outlined in Eqs. (2.16)–(2.21). Table 2 compared the value of $-f''(0)$ with other published results in the literature. In all variations of the magnetic parameter, the numerical values correspond to a reasonable number of decimal places with known results.

4. Result and Discussion

The study of Jeffrey fluid with nonconstant thermal conductivity and chemical reaction over a beeline expanding sheet with anomalous heat flux and mass law is numerically simulated using the following default parametric values for the dimensionless parameters given in Table 3 unless stated otherwise. Figure 2 depicts the impacts of Hartmann parameter on the fluid profiles. The magnetic term introduces additional forces and interactions that can modify the velocity, temperature, and concentration profiles of the fluid. It is noted that the fluid velocity retards with the enhancement of the magnetic force. This behavior is not far-fetched, since the Lorentz force acts as a resistive force to the fluid flow. Physically, the Lorentz force alters the velocity profile by causing the fluid to deviate from its initial path or inducing additional vorticity, thus resulting in a reduction in fluid velocity as the magnetic

Table 3. The thermophysical parametric value.

R	Gr	Gc	Pr	λ_1	ε	θ_w	Λ	ϵ	S_c	Λ_0	Kr	n	β	M	Ec
2.5	0.1	0.1	7.2	0.3	0.5	1.5	0.4	0.2	1.2	1.0	0.2	1.0	0.1	2.5	0.1

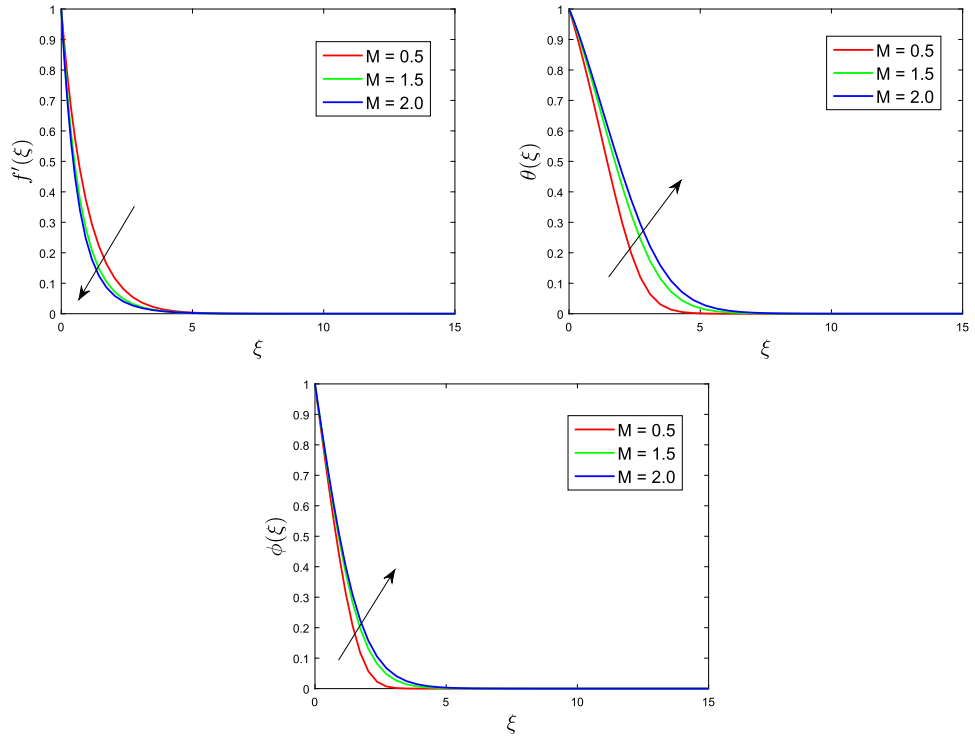

Fig. 2. (Color online) Response of Hartmann number (M) on profile distributions $\frac{\partial f(\xi)}{\partial \xi}$, $\theta(\xi)$, and $\phi(\xi)$.

parameter increases. The enhancement of magnetic force increases both the thermal and solutal boundary layers, respectively. This may be practically accounted for, as the fluid velocity drags slowly over the sheet, more heat is generated at all the gliding contact points of the fluid and the sheet thus, enhancing the temperature distribution profile. Similar findings were reported by Lawal *et al.*[54] for an Erying–Powell fluid flow for the enhancement in the concentration profile — this occurs because the reactive particles in the fluid interact with the magnetic field, leading to boosting of the concentration species profile. Figure 3 shows the influence of R and E_c on $\theta(\xi)$. Increasing the Eckert number results in the generation of heat due to the drag force between the fluid particles which gives rise to the fluid temperature. Similar observation is recorded for the impact of radiation parameter on the $\theta(\xi)$. Physically, thermal radiation is an additional heat source that is introduced into the system. Increasing the heat generation leads to an increment in the temperature profile. The Eckert number represents the ratio of kinetic energy to enthalpy energy. An increase in the Eckert number results in an increase in the heat generation within the fluid, which leads to higher temperature. It is noted that to have a cooling process at a quicker rate, thermal radiation should be minimized. The effects of the chemical reaction parameter and Schmidt numbers are graphically given, respectively, in Fig. 4. The increment in

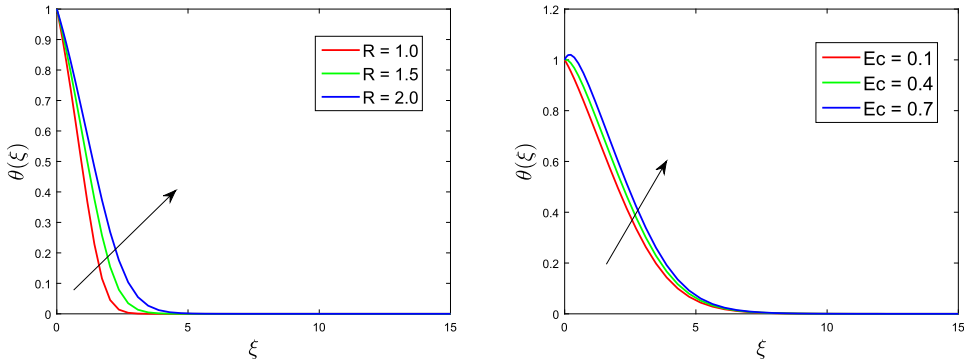

Fig. 3. (Color online) Response of Radiation (R) and Eckert (Ec) parameters on temperature profile distributions $\theta(\xi)$.

the chemical reaction parameter slows down the fluid concentration profiles. This is owing to the fact that the reaction in the system rises with the chemical reaction parameter as the reactant species is consumed in the process thereby reducing the concentration of the fluid. This corroborate the findings of Kasali *et al.*[50]

The increase in the Schmidt number decreases the concentration profiles, this dynamics is synonymous with the impact of chemical reaction parameter. The Schmidt number stands for the ratio of momentum diffusivity to mass diffusivity. A higher Schmidt number implies that the diffusivity of the species is lower relative to the momentum diffusivity. This means that concentration variations will diffuse more slowly. Higher Schmidt number results in slower diffusion of concentration as seen in Fig. 4. Figures 5 and 6 depict the influence of Gr and Gc on the fluid profiles. An increase in the thermal Grashof number leads to the rise in the velocity of the fluid. This shows that the buoyancy force increases with increase in the velocity profile. Natural convection occurs when buoyancy forces dominate the flow, typically due to temperature and concentration differences in the fluid. A higher Grashof

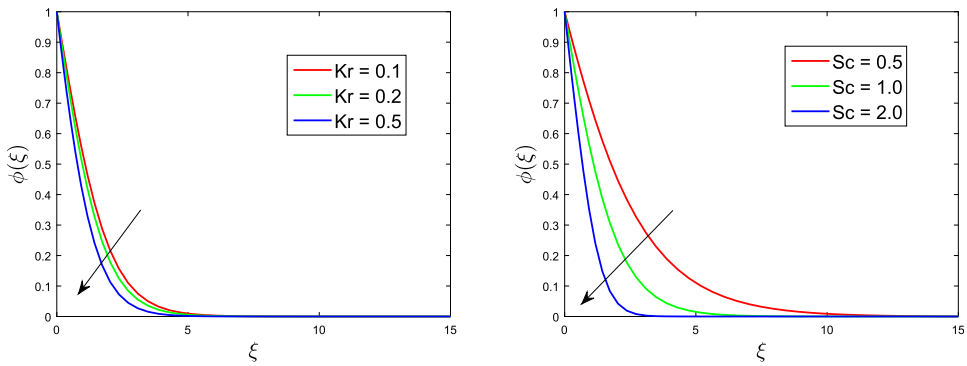

Fig. 4. (Color online) Response of reaction (Kr) and Schmidth (Sc) parameters on concentration profile distributions $\phi(\xi)$.

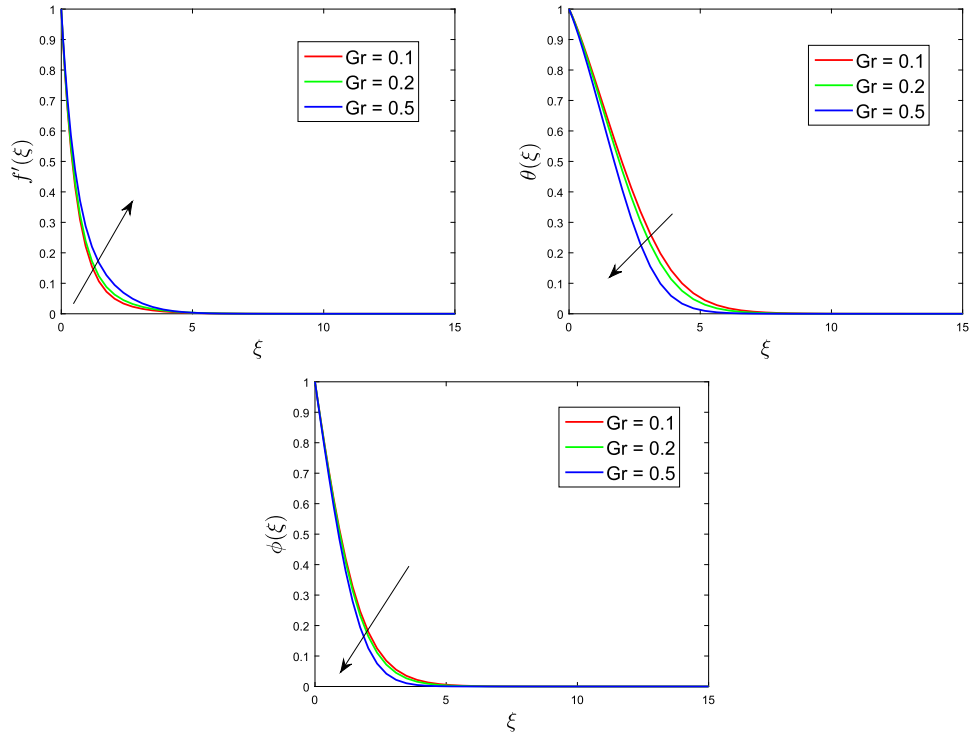

Fig. 5. (Color online) Response of Gr on flow profile distributions $\frac{\partial f(\xi)}{\partial \xi}$, $\theta(\xi)$ and $\phi(\xi)$.

number indicates a stronger buoyancy effect relative to viscous forces. This leads to enhanced fluid motion and mixing, which in turn downsizes the temperature and concentration distributions. For the solutal (modified) Grashof number, an inverse relation exists between the temperature and concentration profiles as the solutal Grashof number increases. The effects of thermal relaxation time, Deborah number and temperature ratio are shown in Fig. 7. Thermal relaxation time shows an inverse

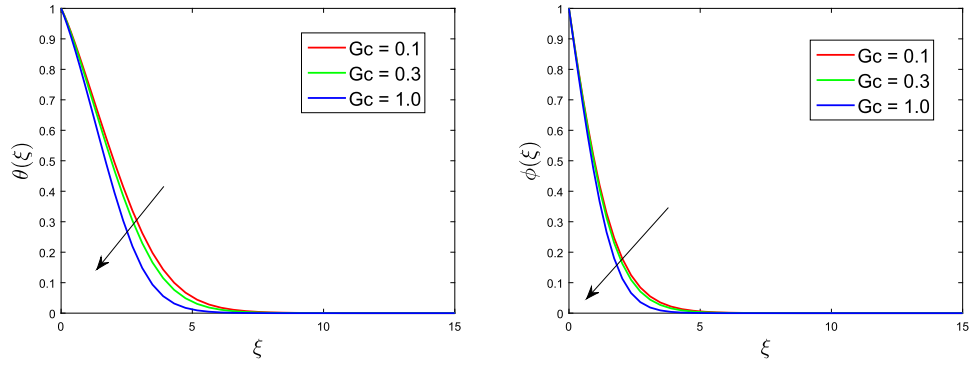

Fig. 6. (Color online) Response of Gc on profile distributions $\theta(\xi)$ and $\phi(\xi)$.

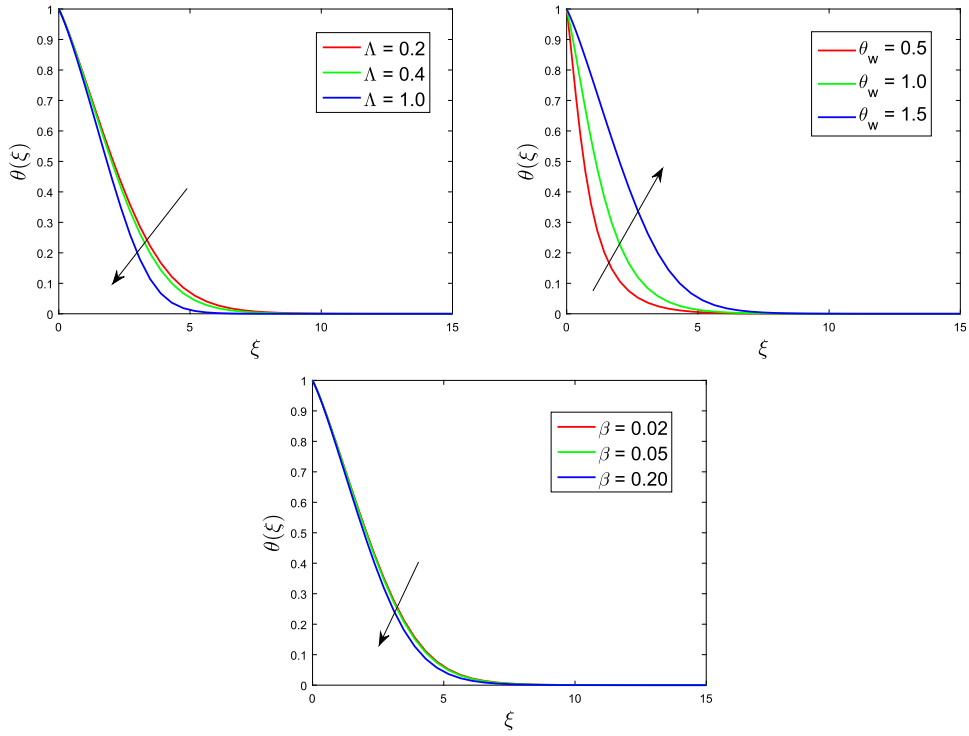

Fig. 7. (Color online) Response of thermal relaxation parameter (Λ), temperature ratio (θ_w) and Deborah number on profile distributions $\theta(\xi)$

relationship with the temperature of the fluid. This is due to the fact that an increment in thermal relaxation time implies heat transfer from one particle to the other takes more time thereby reducing the temperature of the system. The opposing effect is noticed in the case of temperature ratio. An escalating effect of the temperature ratio θ_w on the temperature profile is displayed in Fig. 7. Thus, as the temperature ratio θ_w increases, the temperature profile also increases in behavior as envisaged, being a temperature-associated parameter. Physically, the temperature ratio reflects the strength of the thermal boundary layer, which is the region of the fluid near a solid surface where the temperature varies rapidly due to the heat transfer between the fluid and the surface. The temperature of the fluid reduced with rise in the Deborah number. The Deborah number $\beta = \lambda_2 c$ characterizes the viscoelastic behavior of the fluid. It relates the characteristic time-scale of deformation to the relaxation of the fluid. The viscoelastic behavior of the Jeffery fluid directly affects the temperature profiles by influencing the flow behavior, thus resulting in decreasing temperature distribution as β increases. Deborah number has a direct relationship with the retardation time. The effects of the ratio of relaxation to retardation time λ_1 are shown in Fig. 8.

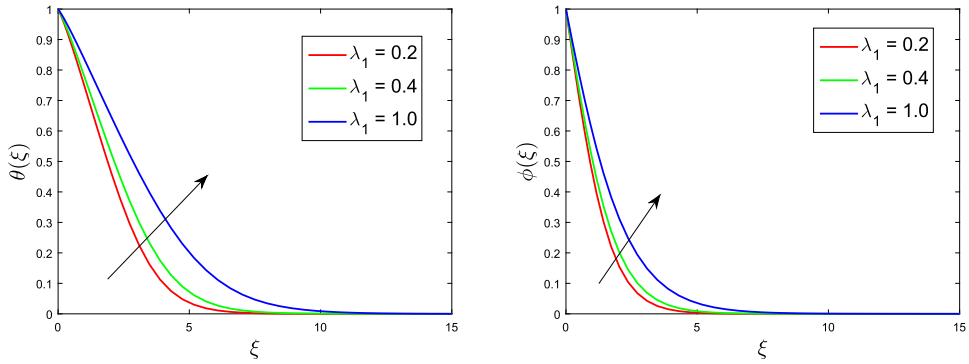

Fig. 8. (Color online) Influence of parameter (λ_1) on the temperature and concentration profiles.

The relaxation time represents the time scale over which the Jeffery fluid returns to its equilibrium state after being subjected to deformation. On the other hand, the retardation time represents the time scale over which the fluid responds to changes in deformation. The viscoelastic properties of the Jeffery fluid, including its ability to store and dissipate energy, influence the flow dynamics, which in turn affect the heat transfer processes. It is observed that temperature and concentration profiles increase with rise in λ_1. The influence of n is presented graphically in Fig. 9. It has been discovered that increasing the parametric value of n has a positive effect on the concentration profile. This suggests that the reaction rate increases with higher concentrations of the reactants.

Table 4 shows the physical quantities (i.e., skin friction, Nusselt and Sherwood number) for the Jeffery fluid flow over an expanding surface. $\frac{1}{2}\mathrm{Re}_x^{\frac{1}{2}}C_f$, $\mathrm{Re}_x^{-\frac{1}{2}}\mathrm{Nu}_x$ and $\mathrm{Re}_x^{-\frac{1}{2}}\mathrm{Sh}_x$ increase with enhancement in radiation, temperature ratio and Grashof parameters. Increasing the Eckert number reduces the skin drag force and $\mathrm{Re}_x^{-\frac{1}{2}}\mathrm{Nu}_x$

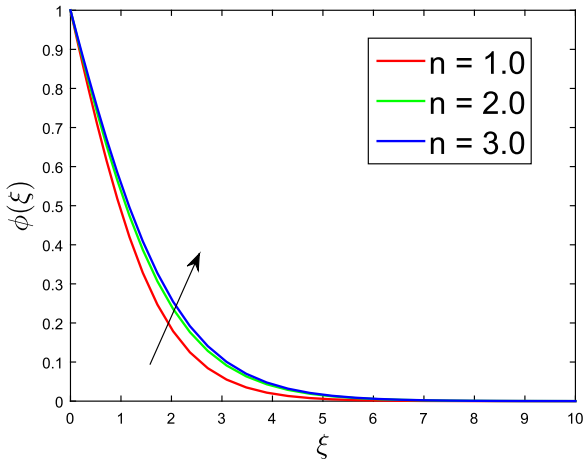

Fig. 9. (Color online) Influence of reaction-order (n) on the concentration profile.

Table 4. Variation in the skin friction, heat and mass transfer rates for parametric values given in Table 3.

Parameters								Physical quantities		
R	β	Gr	E_c	λ_1	ϵ	θ_w	n	$\frac{1}{2}\mathrm{Re}_x^{\frac{1}{2}}C_f$	$\mathrm{Re}_x^{-\frac{1}{2}}\mathrm{Nu}_x$	$\mathrm{Re}_x^{-\frac{1}{2}}\mathrm{Sh}_x$
0.50	0.10	0.10	0.10	0.30	0.50	1.50	1.00	−1.447596	1.429193	0.806648
1.00								−1.443882	1.701763	0.809147
1.50								−1.441541	1.880134	0.811167
2.50	0.10							−1.438835	2.115321	0.813967
	0.15							−1.472094	2.137009	0.818677
	0.20							−1.504631	2.157849	0.823248
	0.10	0.10						−1.438835	2.115321	0.813967
		0.20						−1.401004	2.248285	0.826048
		0.30						−1.363798	2.363418	0.837524
		0.10	0.10					−1.438835	2.115321	0.813967
			0.20					−1.438226	1.255535	0.814320
			0.60					−1.435861	−2.185112	0.815699
			0.10	0.20				−1.559863	2.223875	0.855967
				0.30				−1.438835	2.115321	0.813966
				0.50				−1.245479	1.936738	0.744274
				0.30	0.20			−1.438963	2.154610	0.813829
					0.50			−1.438835	2.115320	0.813966
					0.60			−1.438794	2.102576	0.814011
					0.50	1.00		−1.444186	1.662919	0.809659
						1.50		−1.438835	2.115321	0.813967
						2.00		−1.435682	2.492606	0.817577
						1.50	1.00	−1.438835	2.115321	0.813967
							2.00	−1.437621	2.127779	0.734047
							3.00	−1.437127	2.131914	0.696876

but boosts $\mathrm{Re}_x^{-\frac{1}{2}}\mathrm{Sh}_x$. β downsizes the skin drag force but enhances the heat transfer and mass transfer rate as the value of β grows positively.

5. Conclusion

In accordance with Fourier's law of heat transfer, thermal energy diffuses uniformly throughout the medium. Similarly, Fick's law governs mass transfer at a consistent rate within the medium. However, recent industrial and mechanical applications demonstrate contrasting transport characteristics. Heat and mass transfer are fundamental natural phenomena that occur whenever there exists a temperature/concentration difference between two objects or different regions of the same object. Consequently, understanding and predicting heat/mass transport behavior have been the subjects of extensive research. The uniqueness and structural stability of solutions for energy equations using the Cattaneo–Christov heat flow model and mass equation using the generalized Fick's model have been demonstrated in various initial and boundary value problems. The study here investigated radiative Jeffery fluid flow over a stretched surface with nonconstant thermal conductivity and mass

diffusivity as well as examination of generalized heat and mass flux model. The governing multi-variable differential equations are systematically neutralized into a one-variable differential equations. The spectral SLLM method is used to gain insight into the flow mechanics. Among the findings of this study are the following:

- Enhancement in Eckert number and radiation parameter boosts the thermal boundary layer profile.
- By increasing M, $f'(\xi)$ is dampened while the $\theta(\xi)$ and $\phi(\xi)$ profiles are enhanced.
- A reduction in concentration profiles can be achieved by increasing the Schmidt and chemical reaction parameters.
- By enhancing the Deborah's number, the skin drag force will increase.
- There is an equal correlation between Gr and Gc number over the flow distribution.
- All the graphs presented in this work satisfy the boundary layer phenomenon which signifies that the problem is well posed.

The implementation of the findings from this research work will help regulate the transfer of heat energy and mass flux in various industrial and engineering applications. In future study, the impact of nanoparticles on the Jeffery fluid heat and mass flow behavior as well as influence on the engineering physical quantities will be theoretically investigated. Furthermore, the authors would be interested in exploring the application of this model in different coordinate systems and geometries.

Acknowledgments

The authors are very grateful to the anonymous reviewers who provided detailed feedback to improve this work.

References

1. M. Khan, *J. Porous Media* **10**, 473 (2007).
2. S. V. Jakati *et al.*, *Int. J. Latest Trans. Eng.* **3**, 1 (2018).
3. S. V. Jakati *et al.*, *J. Cent. South Univ.* **21**, 1428 (2014).
4. M. Farooq *et al.*, *J. Mech.* **31**, 319329 (2015).
5. A. Ara *et al.*, *Appl. Comput. Math.* **18**, 135 (2019).
6. A. S. Rao, N. Nagendra and V. R. Prasad, *Procedia Eng.* **127**, 775 (2015).
7. T. Hayat, M. Rafiq and B. Ahmad, *PloS One* **11**, e0145525 (2016).
8. T. Hayat, R. Sajjad and S. Asghar, *Commun. Nonlinear Sci. Numer. Simul.* **15**, 2400 (2010).
9. T. Hayat *et al.*, *Results Phys.* **6**, 817 (2016).
10. S. Bajwa *et al.*, *Math. Probl. Eng.* **9**, (2021).
11. T. Hayat *et al.*, *Hydrol. Hydromech.* **63**, (2015).
12. K. Das, N. Acharya and P. K. Kundu, *Alex. Eng. J.* **54**, 2015 (2015).
13. M. D. Shamsuddin *et al.*, *Waves in Random Complex Media* (2022).
14. M. D. Shamshuddin *et al.*, *J. Magn. Magn. Mater.* **565**, 170286 (2023).
15. F. Asmat *et al.*, *Case Stud. Therm. Eng.* **12**, 271 (2023).

16. D. Yang *et al.*, *Coatings* **11**, 1012 (2021).
17. N. A. Khan *et al.*, *Nonlinear Eng.* **8**, 231 (2019).
18. N. A. Khan, S. Khan and S. Ullah, *AIP Adv.* **5**, 1 (2015).
19. J. H. Merkin, *Math. Comput. Model* **24**, 125 (1996).
20. J. H. Merkin, *Fluid Dyn. Res.* **16**, 311 (1995).
21. N. Bachok, A. Ishak and I. Pop, *Commun Nonlinear Sci. Numer. Simul.* **16**, 4296 (2011).
22. W. A. Khan and I. Pop, *J. Heat Transf.* **134**, 1 (2012).
23. P. K. Kameswaran *et al.*, *J. Heat Transf.* **57**, 465 (2013).
24. M. Israr Ur Rehman *et al.*, *Sci. Rep.* **12**, 18666 (2022).
25. J. B. J. Fourier, *Theorie Analytique De La Chaleur* (Firmin-Didot, Paris, 1822).
26. C. Cattaneo, *Atti Semin. Mat Fis. Univ. Modena Reggio Emilia* **83** (1848).
27. C. I. Christov, *Mech. Res. Commun.* **36**, 481 (2009).
28. M. Israr Ur Rehman *et al.*, *Int. J. Mod. Phys. B* (2020).
29. M. Israr Ur Rehman *et al.*, *Case Stud. Therm. Eng.* **42**, 102737 (2023).
30. S. Z. Alamri *et al.*, *Phys. Lett. A* **383**, 276 (2019).
31. V. Tibullo and V. Zampoli, *Mech. Res. Commun.* **38**, 77 (2011).
32. B. Straughan, *Int. J. Heat Mass Transf.* **53**, 95 (2010).
33. M. Ciarletta and B. Straughan, *Mech. Res. Commun.* **37**, 445 (2010).
34. Y. Dong, B. Y. Cao and Z. Y. Guo, *J. Appl. Phys.* **110**, 063504 (2011).
35. S. Han *et al.*, *Appl. Math. Lett.* **38**, 87 (2014).
36. M. Mustafa, *AIP Adv.* **5**, 047109 (2015).
37. M. B. Ashraf, R. A. Tanveer and S. Ulhaq, *J. Magn. Magn. Mater.* **565**, 047109 (2023).
38. T. Hayat *et al.*, *Int. J. Heat Mass Transf.* **99**, 702 (2016)
39. W. Xiu *et al.*, *J. Magn. Magn. Mater.* **569**, (2023).
40. Y. O Tijani *et al.*, *J. Nanofluids.* **12**, 91 (2023).
41. S. O. Salawu *et al.*, *Res. Materials* **17**, (2023)
42. A. M. Obalalu *et al.*, *Case Stud. Therm. Eng.* **25**, (2023)
43. R. Nischay and S. Mondal, *Partial. Differ. Equ. Appl. Math.* **4**, 100043 (2021).
44. S. Shateyi and G. T. Marewo, *Bound. Value Probl.* **170**, 100043 (2014).
45. S. S. Motsa, *J. Appl. Math.* **13**, 423628 (2013).
46. S. S. Motsa and F. G. Awad, *Abstract Appl. Anal.* 408230 (2014).
47. S. S. Motsa, *Numer. Algorithms* **66**, 865 (2014).
48. H. M. Sithole *et al.*, *Open Phys.* **15**, 637 (2017).
49. V. M. Magagula *Int. J. Math. Sci.* 6423294 (2019).
50. K. B. Kasali *et al.*, *Multidiscip. Model. Mater. Struct.* **16**, 1577 (2020).
51. T. Hayat and S. Nadeem, *Res. Phys.* **7**, 3910 (2017).
52. M. Mustafa, *AIP Adv.* **5**, 047109 (2015).
53. P. V. Satya Narayana and D. H. Babu, *J. Taiwan Inst. Chem. Eng.* **1** (2015).
54. M. O. Lawal *et al.*, *Partial. Differ. Equ. Appl. Math.* **5**, 100318 (2022).
55. M. Ferdous, M. Qasem and Al-Mdallal, *Am. J. Fluid Dyn.* **2**, 89 (2012).
56. K. B. Kasali *et al.*, *Nonlinear Eng.* **11**, 654 (2022).
57. T. E. Akinbobola and S. S. Okoya, *J. Nig. Math. Soc.* **34**, 331 (2015).
58. Y. O. Tijani *et al.*, *Heat Transf.* **51**, 5659 (2022).
59. M. T. Akolade and Y. O. Tijani, *Partial. Differ. Equ. Appl. Math.* 100108 (2021).
60. R. E. Bellman and R. E. Kalaba (Elsevier, New York, 1965).
61. H. A. Ogunseye *et al.*, *Multidiscip. Model. Mater. Struct.* **1**, 1573 (2019).
62. L. N. Trefethen, *SIAM* 10 (2000).
63. A. Alsaedi *et al.*, *Adv Powder Technol.* **28**, 288 (2017).
64. F. Naseem *et al.*, *AIP Adv.* **7**, 065013 (2017).